Heterogeneous Single-Walled Carbon Nanotube Catalyst Discovery and Optimization

Bin Chen,[†] Goldwyn Parker II,[‡] Jie Han,[†] M. Meyyappan, and Alan M. Cassell*,[†]

Center For Nanotechnology, National Aeronautics and Space Administration, Ames Research Center, Moffett Field, California 94035

Received December 7, 2001. Revised Manuscript Received February 7, 2002

High-throughput methods are utilized in the discovery and optimization of heterogeneous catalyst formulations that promote single-walled carbon nanotube (SWNT) synthesis. Catalyst compositions, substrates, and reaction conditions are varied to efficiently investigate SWNT growth by chemical vapor deposition (CVD). A robotic microarray printer is employed to print libraries of the liquid-based catalyst precursors onto various substrates. After CVD, the catalyst arrays are qualitatively screened for yield via electron microscopy. More comprehensive characterization of candidate catalysts is further investigated with confocal Raman spectroscopy (CRS). Detailed CRS mapping reveals information concerning the printed catalyst and nanotube homogeneity in the microarrays. This powerful characterization approach allows for the high-throughput screening of nanotube type, diameter distribution, and purity within the microarrays. The methodology described has enabled the efficient exploration of synthesis parameters, which has led to the identification of SWNT catalysts with various activities.

Introduction

High-throughput experimental methods enable the efficient discovery of genetic markers,[1] new organic compounds,[2] and a variety of materials.[3] Commonly arrayed libraries include nucleic acid probes,[4] proteins,[5] and heterogeneous catalysts.[6−8] Different high-throughput techniques are required depending on the nature of the experiment and the parameter space under investigation. For example, construction and analysis of biochip microarrays requires high-throughput microarray techniques combined with optical-based scanning instruments that process and track the sizable data sets.[9] As combinatorial methodology further develops for nanotechnology applications, increasing reliance on high-throughput screening (HTS) techniques will be needed to analyze the vast amount of information generated. From the viewpoint of developing HTS methodology for heterogeneous catalysts, an important consideration for analysis is the level of detailed characterization that can be obtained from single or multiple HTS instruments. Therefore, the continued utilization of microarrays will require more innovative HTS methodology to enable efficient discovery and optimization.

Different approaches have been used in constructing heterogeneous catalyst[4−8] microarrays, including vapor deposition,[10] ink-jet transfer,[11] and microarray printing.[12] Among these, microarray printing is the most amenable technology for adoption in common laboratories because of its relatively low cost, high spot density ($>10^3$ spots per cm^2), and experimental flexibility. In contrast to high-throughput screening of genetic expression (thousands of probes per microarray), materials screening and optimization are typically performed using smaller numbers of library members. Recently, we extended microarray printing of heterogeneous catalyst precursor inks to explore process variables that influence the growth of multiwalled carbon nanotubes (MWNTs).[13] The size of the printed catalyst precursor microarrays (5 × 5 array size ≈ 2.5 mm × 2.5 mm) allowed for efficient screening via scanning electron microscopy (SEM). Variations in the catalyst compo-

* To whom correspondence should be addressed at NASA Ames Research Center, M/S 229-1, Moffett Field, CA 94035. E-mail: acassell@mail.arc.nasa.gov. Voice mail: (650) 604-2325. Fax: (650) 604-5244.
[†] Eloret Corporation.
[‡] Summer intern from Florida A & M University.

(1) Schena, M.; Shalon, D.; Davis, R. W.; Brown, P. O. *Science* **1995**, *270*, 467.
(2) Merrit, A. T. *Comb. Chem. High Throughput Screening* **1998**, *1*, 57. Thompson, L. A.; Ellman, J. A. *Chem. Rev.* **1996**, *96*, 555.
(3) Jandeleit, B.; Schaefer, D. J.; Powers, T. S.; Turner, H. W.; Wienberg, W. H. *Angew. Chem., Int. Ed. Engl.* **1999**, *121*, 7975. Xiang, X.-D. *Annu. Rev. Mater. Sci.* **1999**, *29*, 149.
(4) Brown, P. O.; Botstein, D. *Nat. Genet.* **1999**, *21*, 33.
(5) MacBeath, G.; Schreiber, S. L. *Science* **2000**, *289*, 1760−1763.
(6) Sun, Y.; Buck, H.; Mallouk, T. E. *Anal. Chem.* **2001**, *73*, 1599.
(7) Cong, P.; Dehestani, A.; Doolen, R. D.; Giaquinta, D. M.; Guan, S.; Markov, V.; Poojary, D.; Self, K.; Turner, H.; Weinberg, W. H. *Proc. Natl. Acad. Sci.* **1999**, *96*, 11077.
(8) Cong, P.; Doolen, R. D.; Fan, Q.; Giaquinta, D. M.; Guan, S.; McFarland, E. W.; Poojary, D. M.; Self, K.; Turner, H. W.; Weinberg, W. H. *Angew. Chem., Int. Ed. Engl.* **1999**, *38*, 484.
(9) Schena, M. *Microarray Biochip Technology*; Eaton Publishing: Natick, MA, 2000.
(10) Danielson, E.; Golden, J. H.; McFarland, E. W.; Reaves, C. M.; Weinberg, W. H.; Wu, X. D. *Nature* **1997**, *389*, 944−948.
(11) Calvert, P. *Chem. Mater.* **2001**, *13*, 3299.
(12) Reddington, E.; Sapienza, A.; Gurau, B.; Viswanathan, R.; Sarangapani, S.; Smotkin, E. S.; Mallouk, T. E. *Science* **1998**, *280*, 1735.
(13) Cassell, A. M.; Verma, S.; Delzeit, L.; Meyyappan, M.; Han, J. *Langmuir* **2001**, *17*, 260−264.

10.1021/cm0116828 CCC: $22.00
Published on Web 03/12/2002

nents and printing parameters affected the spotted film uniformity and, ultimately, the catalyst activity.

From the perspective of SWNT growth, flexibility in catalyst preparation is needed to explore CVD as a synthetic approach for controlling the diameter and type (metallic vs semiconducting) of nanotubes. Achievement of this control is critical to the realization of applications in nanoelectronics and sensors. Techniques such as plasma arc discharge,[14] laser ablation,[15] and continuous gas-phase processes[16] produce SWNT bundles (>10 SWNTs/bundle) with tight diameter distributions. However, the isolation of individual nanotubes requires extensive purification (unwanted impurity removal and debundling) and further processing to obtain material suitable for nanoscale component assembly.[17] Therefore, we have focused on CVD to achieve the goal of synthesizing SWNTs where the yield, density, diameter, and type can be controlled using different heterogeneous catalysts. Without techniques for synthesizing molecularly well-defined nanotubes exclusively and uniformly on patterned surfaces, it is difficult to reproduce and fully realize nanoscale applications of these materials. Therefore, the liquid-phase catalyst precursor discovery and analysis methodology described herein is of general utility for nanomaterials microarrays, and it also sheds light on considerations for optimizing heterogeneous catalysts for carbon nanotube synthesis.

SWNT characterization is traditionally assessed using transmission electron microscopy (TEM) or scanning probe microscopy, techniques that are not very amenable to high-throughput characterization. However, Raman spectroscopy has emerged as a powerful HTS tool for solid-state catalyst materials[18] and pharmaceuticals.[19] Furthermore, Raman analysis of SWNTS has become an extremely powerful technique for studying the chirality, diameter, and one-dimensional properties of SWNTs.[20] Using confocal Raman spectroscopy (CRS), Jorio et al. have shown the tremendous resolving power for the characterization of individual SWNTs.[21] For that reason, fitting the CRS instrument with an automated *XYZ* translation stage can dramatically accelerate the analysis throughput for characterizing catalyst activity within the combinatorial microarrays. Automated array mapping allows for the detailed characterization of SWNTs grown from candidate heterogeneous catalyst formulations. Here, we report the use of CRS, scanning electron microscopy (SEM), and microarray-based catalyst discovery techniques in the exploration and tuning of heterogeneous SWNT catalysts.

(14) Bethune, D. S.; Kiang, C. H.; DeVries, M.; Gorman, G.; Savoy, R.; Vazquez, J.; Beyers, R. *Nature* **1993**, *363*, 605. Iijima, S. *Nature* **1993**, *363*, 60.

(15) Thess, A.; Lee, R.; Nikolaev, Pl; Dai, H.; Petit, P.; Robert, J.; Xu, C. H.; Lee, Y. H.; Kim, S. G.; Rinzler, A. G. Colbert, D. T.; Scuseria, G. E.; Fischer, J. E.; Smalley, R. E. *Science* **1996**, *273*, 483.

(16) Nikolaev, P.; Bronikowski, M. J.; Bradley, R. K.; Rohmund, F.; Colbert, D. T.; Smith, K. A.; Smalley, R. E. *Chem. Phys. Lett.* **1999**, *313*, 91.

(17) Liu, Z.; Shen, Z.; Zhu, T.; Hou, S.; Ying, L.; Shi, Z.; Gu, Z. *Langmuir* **2000**, *16*, 3569.

(18) Stencel, J. M. *Raman Spectroscopy for Catalysis*; van Nostrand Reinhold: New York, 1990.

(19) Pivonka, D. E.; Sparks, R. B. *Appl. Spectrosc.* **2000**, *54*, 1594−1590. Gremlich, H.-U. *Biotechnol. Bioeng.* **1999**, *61*, 179.

(20) Rao, A. M.; Richter, E.; Bandow, S.; Chase, B.; Eklund, P. C.; Williams, K. A.; Fang, S.; Subbaswamy, K. R.; Menon, M.; Thess, A.; Smalley, R. E.; Dresselhaus, G.; Dresselhaus, M. S. *Science* **1997**, *275*, 187.

(21) Jorio, A.; Saito, R.; Hafner, J. H.; Lieber, C. M.; Hunter, T. McClure, G. Dresselhaus, M. S. Dresselhaus, *Phys. Rev. Lett.* **2001**, *86*, 1118.

Experimental Procedure

Materials and Reagents. $AlCl_3 \cdot 6H_2O$, $CoCl_2 \cdot 6H_2O$, $Fe(NO_3)_3 \cdot 9H_2O$, $Si(OEt)_4$, ethanol, and methanol from Sigma-Aldrich Corporation; N-doped silicon wafers (⟨100⟩, 1−10 Ω cm) from Wafer World Inc. (West Palm Beach, FL); aluminum, molybdenum, and iridium (99.99% purity) from Alfa Aesar Inc.; and argon (99.999% Scott Specialty Gas), methane (99.999% Matheson Gas Products), and P-103 triblock copolymer from BASF Inc. (Mount Olive, NJ) were used in this study.

Catalyst Solution Preparation. A typical preparation of a stock catalyst solution follows. First, 0.5 g (0.09 mmol) of Pluronic P-103 triblock copolymer was dissolved in 15 mL of a 2:1 mixture of ethanol and methanol. Next, tetraethyl orthosilicate (1.67 mL, 7.5 mmol) was added to the triblock copolymer/alcohol solution, and the mixture was stirred for 30 min at room temperature. Stock solutions of $AlCl_3 \cdot 6H_2O$, $CoCl_2 \cdot 6H_2O$, and $Fe(NO_3)_3 \cdot 6H_2O$ were prepared at the same concentration of structure-directing agent (SDA) and inorganic salts. The catalyst precursor solutions were filtered through 0.45-μm poly(tetrafluoroethylene) membranes (Osmonics Inc.) prior to printing. The catalyst precursor ink libraries were then prepared by mixing the stock solutions in varying ratios directly in the wells of the 384-well microplates. The ink-loaded microplates were then sealed with paraffin film and vigorously vortexed for 5 min to ensure uniform precursor composition.

Catalyst Printing. In a typical printing, the coated substrates were placed in the robotic microarrayer (SpotBot, TeleChem Inc., www.arrayit.com), and printing was performed with a center-to-center spot spacing of 325 μm. Roughly 1 nL of catalyst solution was transferred per printing, with spot diameters between 100 and 200 μm. After the microarray printing was complete, the stainless steel pins were sonicated for 30 min in methanol to remove any clogging or impurities from the pin. The pins were checked using an optical microscope prior to reinsertion in the robotic print head. Because some of the inorganic salts are corrosive, rapid removal and cleaning of the pins after completion of the printing was necessary to maintain the lifetime and print reproducibility of the individual pins.

Growth Substrates. Ion-beam-sputtered films of Al, Ir, and Mo were prepared on Si(110) using a model TM 200s Ar ion beam sputterer (VCR Group, Inc.) Al and Ir underlayer thicknesses were varied between 10 and 30 nm, and Mo layer thicknesses were varied between 1 and 10 nm.

Chemical Vapor Deposition. The printed chips were loaded into a 1-in.-diameter tube furnace (Lindbergh Blue) and heated to 400 °C for 12 h under flowing air to render the catalyst precursors active (i.e., to decompose the inorganic salts and remove the SDA). This calcination process converts the inorganic salts into metal oxides. For simplicity, we refer to catalyst compositions solely on the basis of the cations present in the catalyst mixtures. Methane flow rates between 100 and 5000 sccm (MKS Instruments mass flow controllers) and deposition temperatures between 850 and 950 °C were investigated. Reaction times were varied between 5 and 40 min, but the typical reaction time for the discovery process was 20 min.

Electron Microscopy. The reacted chips were examined using a Hitachi S-4000 field emission scanning electron microscope operating between 15 and 30 kV accelerating voltage. The SEM was equipped with an *XYZ* translation stage that allowed for precise movement. Qualitative scanning of the yield was typically performed in less than 1 h for discovery libraries and in 1.5 h for focus libraries. TEM analysis was performed (JEOL 200CX instrument operating at 200 kV) on candidate catalysts by scaling-up the catalyst to obtain enough NT sample for conventional TEM analysis. Scale-up involved forming thin films of the catalyst precursor (0.5 μL via pipet) on the substrate (1 cm^2) using spin-coating (600 rpm) and then performing NT growth. Material was scraped off the sub-

strates, ultrasonicated in methanol for 10 min, and then deposited onto carbon-film-coated TEM specimen grids.

Confocal Raman Spectroscopy. Raman spectra were collected using a System 2000 micro-Raman spectrometer (Renishaw Inc.) in the backscattering configuration. Nanotubes derived from candidate catalysts were analyzed using 4−5 mW laser power with focused laser spot sizes of 1, 5, or 10 μm for the different objectives. The majority of the spectra were collected at 50% laser power and 10-s accumulation time when the 50× objective was used (∼1 μm beam spot). Spectral stitching is not required for this instrument for the spectral window 0−4000 cm^{-1}. We employed an excitation source of 785 nm (1.58 eV) and focused our analysis within the spectral window (100−2000 cm^{-1} , 4 cm^{-1} resolution in this configuration). The spectrometer was calibrated with atomic emission from a neon lamp and referenced to silicon lines (303, 520, and 960 cm^{-1}) before the spectra were collected. Spectra were collected from three different areas in each catalyst spot to ensure reproducibility for peak intensities. We assumed that our samples contained randomly oriented NTs and that we obtained average characteristic spectral information using SEM correlations. Promising candidate catalysts can be extensively mapped using the automated CRS mapping feature. During mapping, the 20× objective in conjunction with the automated *XYZ* translation stage was used for detailed mapping analysis. The software interface allows for precise control of the *XYZ* sample translation stage, which can be positioned to collect spectra from predesignated areas within the microarrays or individual catalyst spots. The mapping software simultaneously records the *XY* position and the corresponding spectra from the sample. *XY* stepping of 5 μm/step was utilized for the detailed mapping of a single catalyst spot in as few as 6 h (120 μm × 120 μm analysis area, total of 576 spectra). Less detailed mapping analysis (NT screening) of the catalyst microarrays can be carried out in less than 1 h (3 spectra/catalyst spot, total of 25 catalyst spots). The mapping data are obtained by software comparison of the measured spectra to a referenced spectrum, with the comparisons based on the differences between the peak spectral features (intensity, peak position, and shape).

Results and Discussion

Previous investigations of heterogeneous SWNT catalysts have revealed certain physical and chemical requirements for achieving high-yield growth. For thermal CVD, the optimal catalyst should have strong metal−support interaction, an open textural structure (high surface area and optimal pore size distribution), and an active support surface (Lewis acid sites) that allows for efficient hydrocarbon breakdown.[22] For CVD using methane, the most active metals for SWNT synthesis appear to be Fe nanoparticles with a small amount of Mo as a cocatalyst, and the amount of Mo can be varied to control the density of SWNT growth.[23] We chose the catalyst precursor inks and print substrates with this in mind. The precursor inks consist of a removable pore-forming agent, Pluronic P-103 [triblock copolymer, poly(alkylene oxide)] that serves as a SDA[24] as well as a wetting agent for uniform film printing of the microarrays on metal surfaces. Previous investigations have shown that these SDAs lead to metal oxide materials with surface areas of >300 m^2/g and pore size distributions mainly in the mesopore range (2−50 nm). For the chemical components of the discovery library, we chose Al, Co, Si, and Fe salts for the rapid identification of active chemical formulations for CH_4-based SWNT CVD.

Scheme 1. Discovery and Optimization Process Schematic Flow[a]

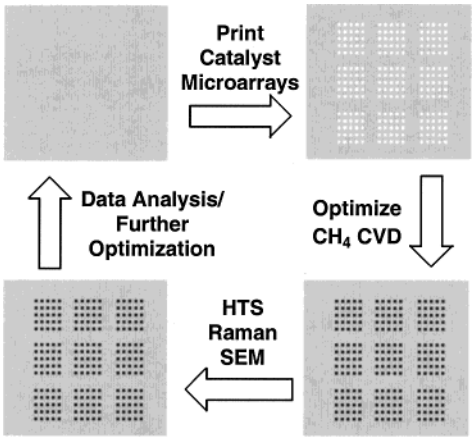

[a] Printing of the catalyst microarrays, followed by CVD, high-throughput screening, and data analysis for further tuning of the catalysts and reaction conditions.

Scheme 1 illustrates our basic approach for SWNT catalyst optimization. Discovery library microarrays were printed in a 5 × 5 array format on different growth substrates for the rapid assessment of reaction conditions, catalyst compositions, and substrate combinations useful for SWNT growth. Previously, we had found that ion-beam-sputtered metal layers composed of Al, Fe, and Mo (<30 nm) are useful for promoting and controlling the density of NT growth on silicon, quartz, and carbon substrates.[25] From this study, we identified two metal underlayers useful for promoting SWNT growth using CH_4 (Al) and MWNT growth using C_2H_4 (Ir). During the SWNT discovery library print substrate optimization, we found that an underlayer composition of 30 nm of Al below 2 nm of Mo gave the highest yield of SWNTs. For the printed inks, our first goal was to optimize the yield (activity) and to find the optimal chemical composition space for the discovery library rapidly. After CVD, the discovery libraries were qualitatively examined using SEM to evaluate catalyst uniformity and SWNT yield. Figure 1 lists the discovery library stoichiometry and spot locator for each catalyst precursor. A low-magnification SEM image of the discovery library microarray after SWNT growth is shown in Figure 2a. The size difference of the printed catalyst spots is due to differences in the print-tip dewetting and substrate wetting properties of the precursor inks.[26]

The initial qualitative evaluation of SWNT yield is illustrated in Figure 2. The optimal reaction conditions were a furnace temperature of 900 °C and a CH_4 flow rate of 1500 sccm. On average, each 25-member microarray was analyzed in 1.5 h using low- (40×) and high-magnification SEM (50k×), which allowed for quick identification of the most active region in the microarrays. The region of highest SWNT yield identified by SEM is outlined in white (Figure 2a). Spots 13,

(22) Cassell, A. M.; Raymakers, J. A.; Kong, J.; Dai, H. *J. Phys. Chem. B* **1999**, *103*, 6484.
(23) Su, M.; Li, Y.; Maynor, B.; Buldum, A.; Lu, J. P.; Liu, J. *J. Phys. Chem. B* **2000**, *104*, 6505. Li, Y.; Liu, J.; Wang, Y.; Wang, Z. L. *Chem. Mater.* **2001**, *13*, 1008.
(24) Yang, P.; Deng, T.; Zhao, D.; Feng, P.; Pine, D.; Chmelka, B. F.; Whitesides, G. M.; Stucky, G. D. *Science* **1998**, *282*, 2244.
(25) Delzeit, L. D.; Chen, B.; Cassell, A.; Stevens, R.; Nguyen, C.; Meyyappan, M. *Chem. Phys. Lett.* **2001**, *348*, 368.
(26) Fondecave, R.; Wyart, F. B. *Macromolecules* **1998**, *31*, 9305.

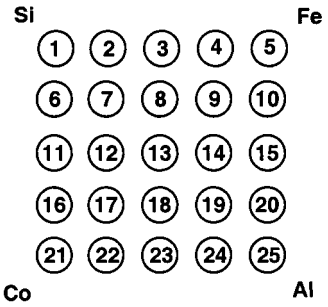

Spot #	Composition	Spot #	Composition
1	Si	14	$SiFe_3Al_2Co$
2	Si_3Fe	15	AlFe
3	SiFe	16	$SiCo_3$
4	$SiFe_3$	17	$SiFeAlCo_3$
5	Fe	18	$SiFeAl_2Co_2$
6	Si_3Co	19	$SiFeAl_3Co$
7	$Si_3FeAlCo$	20	$FeAl_3$
8	Si_2Fe_2AlCo	21	Co
9	$SiFe_3AlCo$	22	$AlCo_3$
10	Fe_3Al	23	AlCo
11	SiCo	24	Al_3Co
12	$Si_2FeAlCo_2$	25	Al
13	SiFeAlCo		

Figure 1. Discovery library composition table and spot locator.

14, and 18−20 were found to have an apparent high SWNT yield as determined by SEM. SEM images of spot 13 (SiFeAlCo) and spot 19 ($SiFeAl_3Co$) are shown in Figure 2b,c. Unwanted impurities such as amorphous carbon, MWNTs, and graphitic particulates are difficult to characterize using SEM. The presence of SWNTs by SEM was determined on the basis of the absence of many defects along the nanotube lengths. However, the limited resolution of SEM (∼5 nm) is unable to truly resolve the nanotube type (single- vs multiwalled) or the extent of nanotube bundling (average number of SWNTs per bundle). Some of the formulations found to be less active in the discovery array exhibited signs of SWNTs but were also found to contain MWNTs (kinks and large-diameter tube structures, >30 nm, data not shown). Further elucidation of the nanotube distribution within each spot in the microarrays was done using CRS.

A focus library was then constructed with spots 13, 14, 18, and 19 from the discovery library serving as corners of the 5 × 5 focus microarray. The focus microarray was reacted using the optimized growth conditions found for the discovery library (900 °C, 1500 sccm CH_4). Verification of SWNT yield was made using high-resolution SEM before detailed CRS analysis was initiated. Catalyst spots identified as producing MWNTs and defective fibrous material by SEM were analyzed using CRS for comparison to spots predominantly producing SWNTs (Figure 3). Comparison of the Raman scattering (785-nm excitation) data generated from spots shown to produce MWNTs indicates two broad peaks centered at 1320 cm^{-1} (D band) and 1590 cm^{-1} (G band). As extensively discussed in the literature,[27] peak presence, relative peak intensities, and peak breadth are indicators of NT type. The D-band peak can be attributed to three possible carbon types: nanotubes with open caps, wall defects, or amorphous carbon introduced in the growth process. Typically, the D-band peak is substantially more intense when MWNTs are present. For a characteristic MWNT spectrum obtained from the catalyst microarrays (Figure 3, bottom spectrum), the D-band peak intensity is just above that of the G band, and we see no appreciable peaks in the radial-breathing-mode region (RBM, 100−400 cm^{-1}). A typical SWNT spectrum (Figure 3, top spectrum) shows characteristic signatures of SWNTs, namely the characteristic narrow G band with a much less intense

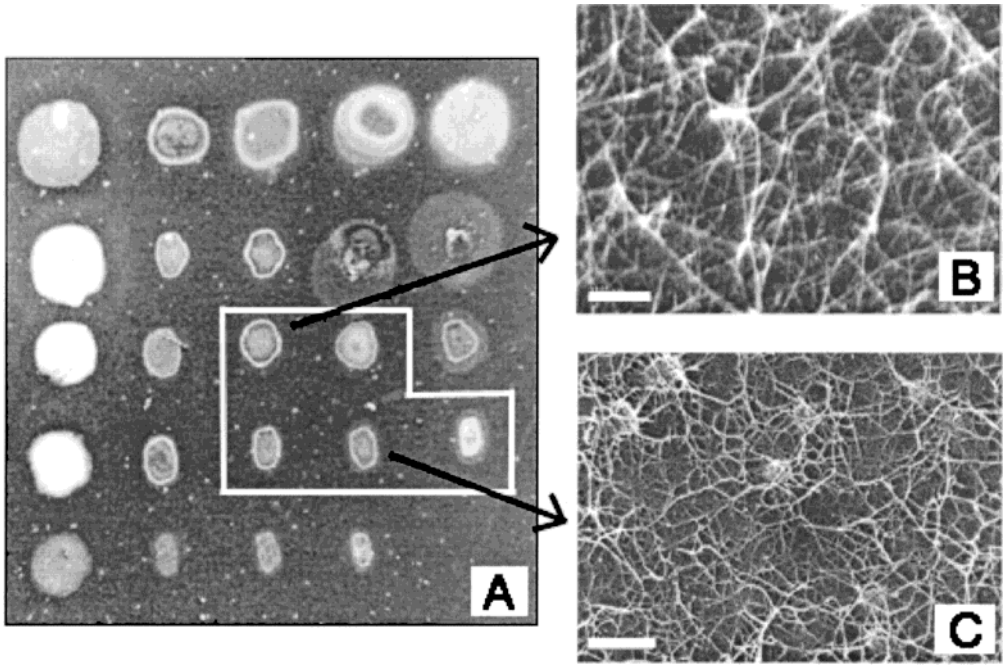

Figure 2. (a) Low-magnification SEM image of the discovery library microarray after SWNT growth. The most active SWNT catalysts identified by SEM are outlined in white (spots 13, 14, and 18−20). (b) High-magnification SEM image of spot 13 (scale bar = 200 nm). (c) High-magnification SEM image of spot 19 (scale bar = 300 nm).

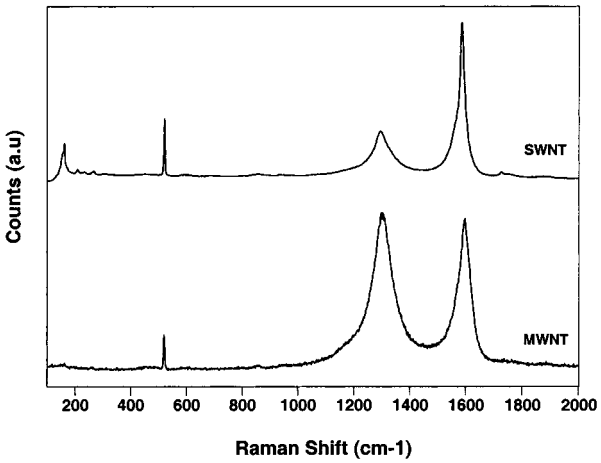

Figure 3. Raman spectra comparison for catalysts identified as mainly producing MWNTs or SWNTs as correlated with high-magnification SEM imaging. Typical signatures of MWNTs and SWNTs are discussed in the text.

D-band peak. Other less intense features in the RBM region and a secondary combination band at 1730 cm^{-1} are further evidence of the presence of SWNTs. Assignments for SWNT diameters that resonate with 785 nm (1.58 eV) excitation can be calculated using the following formula

$$\Omega_{RBM}\ (cm^{-1}) = \alpha/d\ (nm) \qquad (1)$$

where $\alpha = 248\ cm^{-1}$ and Ω is the Raman shift.[19] Solving for d, we obtain SWNT diameters ranging between 0.9 and 1.7 nm.

Similarity mapping of catalyst spots from the focus library was performed to further investigate SWNT catalyst homogeneity within each spot in the microarray. Mapping of the SWNTs was performed using 785-nm excitation because many SWNTs resonate well at longer excitation wavelengths.[21] This allows us to perform automated, detailed analysis of the nanotube distribution and, thus, the catalyst uniformity. When manual sample collection is used, much better beam focus is obtained, but detailed examination is often very user-oriented and can result in poor data interpretation. The automated *XYZ* stage allows for the precise movement and positioning of the beam for the desired analysis detail required. This feature removes many of the experimental variables that can lead to poor data reproducibility. One complicating factor for interpretation of the mapping data is the relative bundle size and density of SWNTs. Therefore, electron microscope examination is extremely useful for correlating the data obtained by CRS. In the high-yielding catalyst spots from the focus library, we typically see SWNT densities of >10 SWNTs/μm^2. Typical mapping results (spot 5, focus library, $SiFe_3Al_2Co$) are shown in Figure 4. Using the automated mapping feature, we can examine the sample homogeneity at the microscopic level. For example, the mapping datum (Figure 4a) is generated at each pixel by calculating the relative difference from the reference spectrum (typical SWNT spectrum, Figure 4b). The darker areas (black) in the map represent spectra

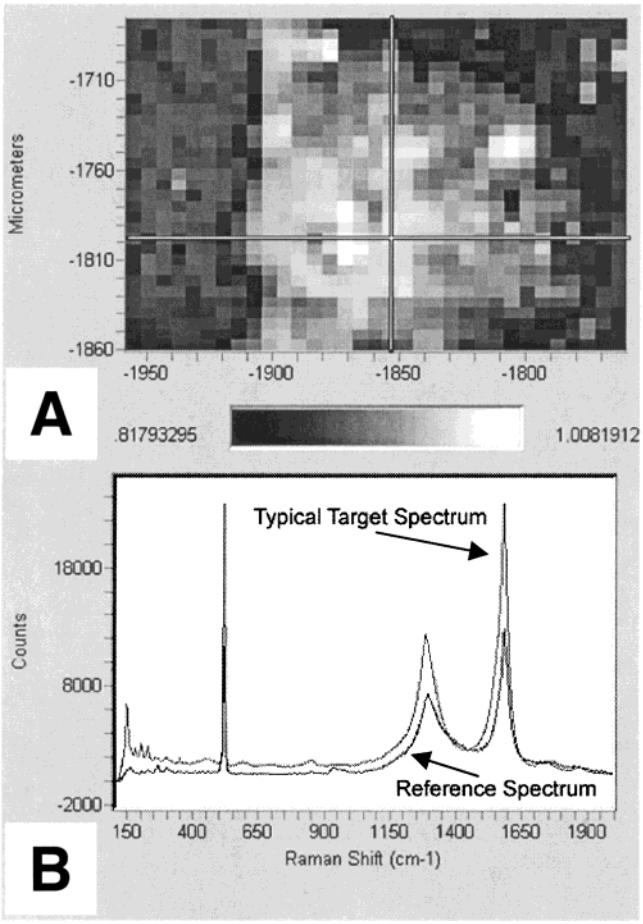

Figure 4. (a) Similarity map for spot 5 from the focus library showing the relative nanotube homogeneity throughout the catalyst spot. A comparison of each pixel collected to the corresponding location on the reference spectrum generates a similarity map that shows the relative homogeneity distribution across the catalyst spot. (b) Reference spectrum (shown at the bottom) that was used to generate the similarity map, with a typical spectrum within the catalyst spot. Mapping analysis was performed using the 20× objective.

whose values are significantly lower in peak intensity or have no spectral similarity at all with the chosen reference spectrum, whereas the lighter pixels (white areas) represent spectra whose values exhibit larger relative peak intensities than the reference spectrum (as shown in Figure 4b). Grey pixels represent areas that more closely match the reference spectrum. The catalyst spot outline can be seen in the mapping image and shows the relative extent of NT homogeneity. The mapping data correlates well with high-resolution SEM imaging of the same catalyst spot. The catalyst spots in the focus library show similar SWNT distribution mapping analysis features, namely, a general trend toward poor homogeneity. The difference mapping suggests that obtaining uniform nanotube distribution across the printed catalyst spot remains a distinct challenge.

Comparing the RBM regions of the different catalyst formulations allows for further detailed examination of SWNTs made from these catalyst arrays. The RBM region contains valuable information about SWNT diameter and type based on the Raman shift. However, we limit our discussion here to demonstrating the instrument's resolving power using only one excitation

(27) Saito, R.; Dresselhaus, G.; Dresselhaus, M. S. *Physical Properties of Carbon Nanotubes*; Imperial College Press: London, 1998.

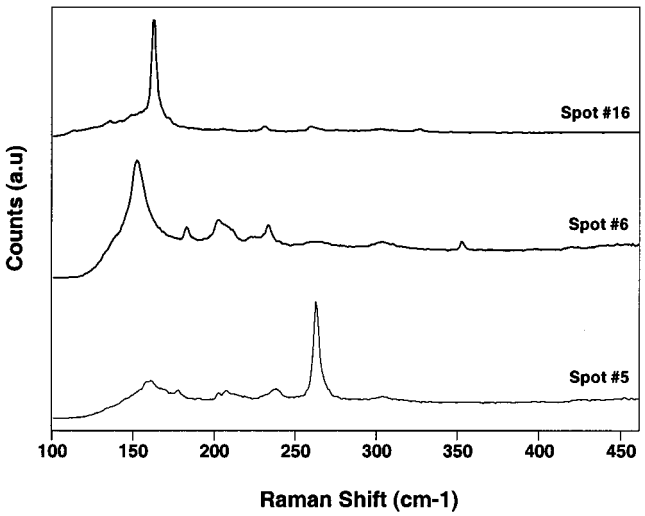

Figure 5. Comparison of the radial-breathing-mode region between three different catalyst spots from the focus library shows the relative distribution of SWNT diameters. Different catalysts give different diameter distributions.

source. We find significant SWNT distribution differences between catalyst spots, although a multiple-excitation-source study is needed for further diameter distribution analysis. Inspection of the Raman spectra (Figure 5) reveals that different chemical formulations give rise to different distributions of observed SWNT diameters. Although the distributions of peaks in the RBM region are slightly different between spots, the total intensity remains relatively unchanged. For each catalyst spot, we analyzed three different regions within the spot to ensure spectral reproducibility. Again, using eq 1, we calculated the SWNT diameter distribution, which ranged from 0.9 to 1.63 nm in the three spots (5, 6, and 16). The diameter distributions produced with different catalysts were quite distinct (Figure 5). Spot 16 ($Si_5Fe_8Al_8Co_8$, focus library) gave a prominent peak at 162 cm^{-1}. Spots 5 ($SiFe_3Al_2Co$) and 6 ($Si_7Fe_8Al_8Co_8$) also each gave a single dominant peak (264 and 148 cm^{-1}, respectively), but their spectra also contain less intense peaks distributed throughout the region. The diameter distribution of SWNTs derived from heterogeneous catalysts can vary depending on the catalyst composition and homogeneity in the printed spot. One complicating factor in the comparison of the RBM region for different catalysts is the average SWNT bundle size. However, we find that, on average, different catalyst compositions lead to different SWNT diameter distributions. Therefore, we hesitate to rank the catalysts purely on the basis of a combination of CRS and electron microscopic data. Ultimately, the methodology enables the researcher to tailor the properties of the catalyst and, therefore, the final synthesized nanomaterials for the particular application of interest.

Concluding Remarks

We have identified active catalysts for growing SWNTs using the liquid-phase precursor approach. Stoichiometries of the general formula $Si_xFe_yAl_aCo_b$ (where $x \approx 1$, $y \approx 1.5$, $a \approx 2$, and $b \approx 1$) were found to give SWNTs of varying diameter distributions. The stoichiometry of the highly active spots in the discovery library is similar to compositions previously identified as active catalysts for hydrocarbon-based CVD.[22,28] The nature of this observation might be due to the total amount of Fe present in the multicomponent catalyst. Although Co is found to be relatively inactive for SWNT growth under these reaction conditions, it could serve as an alloy-forming metal that helps "dilute" the Fe. This observation is currently being studied in more detail. The use of heterogeneous catalysts for CVD-based SWNT growth shows great promise for controlling different aspects of SWNT synthesis through further catalyst engineering that will aid in large-scale nanodevice assembly. Films spun from these liquid-phase precursors could be useful for large-scale patterning on microfabricated substrates.

SWNT catalyst optimization will continue to rely on the implementation of HTS tools and other synthesis platforms that allow for further analysis and selectivity tuning. One drawback to these types of catalyst precursor inks is the lack of homogeneity in the catalyst spots due to differences between the surface properties of the different components in the printed inks. Print spot drying, inorganic salt solubility, and chemical stability are all considerations for further study. Further study is also needed to confirm the chemical composition homogeneity and the relative distribution of SWNTs across the catalyst spot using more detailed mapping analysis. CRS was found to be a valuable HTS platform in this investigation. Further Raman study on the printed catalyst precursors before growth is needed to shed more light on the catalytic activity of the printed spots to establish a fundamental basis for homogeneity issues under consideration. Continued improvements in high-throughput methodology will undoubtedly accelerate the speed at which nanotechnology applications will be realized.

Acknowledgment. We thank A. M. Rao, K. McGuire, and Z. Chi for informative discussions. The National Cancer Institute's Unconventional Innovations Program and NASA Ames Center for Nanotechnology supported this work. Eloret Corp. authors were supported by a NASA contract (NAS2-99092).

CM0116828

(28) Kukovecz, A.; Konya, Z.; Nagaraju, N.; Willems, I.; Tamasi, A.; Fonseca, A.; Nagy, J. V.; Kirisci, I. *Phys. Chem. Chem. Phys.* **2000**, *13*, 3071.